

# Galaxy clustering in the Herschel deep field

H. J. McCracken<sup>1,3</sup>, T. Shanks<sup>1</sup>, N. Metcalfe<sup>1</sup>, R. Fong<sup>1</sup>  
 A. Campos<sup>1,2</sup>

<sup>1</sup>Department of Physics, University of Durham Science Laboratories, South Rd, Durham DH1 3LE.

<sup>2</sup>Instituto de Matemáticas y Física Fundamental (CSIC) Serrano 113 bis, E-28006 Madrid, Spain

<sup>3</sup>Present address: Laboratoire d’Astrophysique de Marseille, 13376 Marseille Cedex 12, France

27 October 2018

## ABSTRACT

We present a study of the angular correlation function as measured in the William Herschel Deep Field, a high galactic latitude field which has been the subject of an extensive observing campaign from optical to infrared wavelengths. It covers 50 arcmin<sup>2</sup> and with it we are able to investigate the scaling of the angular correlation function to  $B \sim 28$ ,  $R, I \sim 26$ ,  $K \sim 20$  and  $H \sim 22.5$ . We compare our measurements to results obtained from the smaller Hubble Deep Field. To interpret our results, we use a model which correctly predicts colours, number counts and redshift distributions for the faint galaxy population. We find that at fixed separation the amplitude of  $\omega(\theta)$  measured in *BRI* bandpasses is lower than the predictions of a model containing with no luminosity evolution and stable clustering growth in proper co-ordinates. However, in the near-infrared bandpasses, our measurements are consistent with the predictions of an essentially non-evolving  $K$ – selected galaxy redshift distribution. In the range  $B \sim 27 - 28$  we find that our correlation amplitudes are independent of magnitude, which is consistent with the observed flattening of the number count slope and correspondingly slower increase of the cosmological volume element expected at these magnitudes.

If our luminosity evolution models provide a correct description of the underlying redshift distributions (and comparisons to available observations at brighter magnitudes suggest they do), then our measurements in all bandpasses are consistent with a rapid growth of galaxy clustering ( $0 < \epsilon < 2$  in the normal parametrisation) on the sub-Mpc scales which our survey probes. We demonstrate that this rapid growth of clustering is consistent with the predictions of biased models of galaxy formation, which indicate that a rapid rate of clustering growth is expected for the intrinsically faint galaxies which dominate our survey.

## 1 INTRODUCTION

The projected two-point galaxy correlation function  $\omega(\theta)$  has proved to be one of the most enduring statistics in observational cosmology. This is a consequence of the relative ease with which it may be measured; for each galaxy, all one requires is positions and magnitudes. Starting with the early studies of clustering in the local universe using Schmidt plates (Groth & Peebles 1977) to more recent works using CCD-based detectors (Efstathiou et al. 1991; Pritchett & Infante 1992) these studies have probed galaxy clustering to very faint magnitudes. Normally, these surveys measure how the amplitude of the projected angular correlation function at a fixed angular separation,  $A_\omega$ , varies as a function of sample limiting magnitude – the “scaling relation”. Usually, this relation has been parametrised in terms of “epsilon models” in which the three-dimensional correlation length  $r_0(z)$  scales monotonically with redshift (Groth & Peebles 1977; Phillipps et al. 1978). These models also require a choice of

cosmology and knowledge of the underlying redshift distributions for each magnitude-limited sample.

In this paper we will investigate the projected angular clustering of the faint field galaxy population. We characterise galaxy clustering as a function of sample limiting magnitude in *BRIKH* bandpasses. Our primary dataset is a deep, ground based survey of an area called ‘the William Herschel deep field’ (WHDF). This has been described in several recent papers (Metcalfe et al. 1996; McCracken et al. 2000). Covering  $\sim 50$  arcmin<sup>2</sup> this survey comprises an area  $\sim 10$  times larger area than the separate HDF-N and HDF-S fields. For comparison, we also present a complementary analysis of clustering amplitudes measured in these smaller fields, utilising the catalogues produced in Metcalfe et al (2000). Although similar studies of  $\omega(\theta)$  exist in the literature (Efstathiou et al. 1991; Roche et al. 1993; Brainerd, Smail, & Mould 1994; Hudon & Lilly 1996; Woods & Fahlman 1997) our survey differs primarily in its depth

( $B \sim 28$ ) and broad wavelength coverage (in this analysis we consider samples selected in *BRIK* bandpasses).

To interpret our results we use redshift distributions derived from the luminosity evolution models we have described in our previous papers ((McCracken et al. 2000; Metcalfe et al. 1996). These models are able to reproduce all the observable quantities of the faint field galaxy population (counts, colours, redshift distributions), at least for low  $\Omega_0$  universes and within current observational uncertainties (Metcalfe et al. 1996); it is these successes which give us confidence in using our models as probe of the clustering history of the Universe, rather than using our measurements of  $A_\omega$  as a probe of the underlying redshift distributions. In our models, high  $\Omega_0$  Universes can be accommodated by the model if we add an extra population of low luminosity galaxies with constant star-formation rates which boost the counts at faint ( $B > 25^m$ ) magnitude levels (Campos 1997). We also consider flat cosmologies with  $\Lambda \neq 0$ . For reference, the scaling relation computed for a model with stable clustering and no luminosity evolution is also presented.

Models such as those presented in this paper are relatively successful in describing clustering measurements performed on deep blank-field surveys like the one detailed in this work (Roche et al. 1993; Brainerd, Smail, & Mould 1994). However, observations of the clustering properties of Lyman-break galaxies (Madau et al. 1996) indicate that these objects have comparable clustering properties (Giavalisco et al. 1998) to some classes of locally observed galaxies, making such objects initially difficult to understand in terms of this monotonic scaling of  $r_0$  with redshift. We will explain how these observations can be understood in the context of the results presented in this paper.

Our paper is organised as follows: in Section 2 we describe in outline the preparation of our datasets; in Section 3 we describe the techniques we use to measure and analyse our data; in Section 4 we present our measurements of the projected correlation function in five bandpasses in comparison with previous work and investigate if our errors estimates are realistic; in Section 5 we compare our correlation measurements with the predictions of our evolutionary models; and finally, in Section 6 we outline the main conclusions from this work.

## 2 OBSERVATIONS AND CATALOGUES

Full details of the optical observations comprising the WHDF will be presented in a forthcoming paper (Metcalfe et al 2000). A subset of our infrared observations of the WHDF is described in McCracken et al. (2000) which comprises the  $K < 20$  UKIRT observations. Additional infrared observations at Calar Alto Observatory produced a second catalogue limited at  $H < 22.5$  which will be fully described in a separate paper (McCracken et al, in preparation). In this section we will briefly describe our object detection and photometry techniques which are very similar to that used in our previous galaxy counts papers (Metcalfe et al. 1991; Jones et al. 1991; Metcalfe et al. 1995; McCracken et al. 2000). All our optical data discussed in this paper was taken at the William Herschel Telescope (WHT), with the exception of a short  $I$ -band exposure made at the Isaac Newton Telescope (INT).

After bias subtraction and flat-fielding, the sky background is removed and isophotal image detection is carried out. These images are then removed from the frame, replaced by a local sky value, and the resulting frame smoothed heavily before being subtracted from the original. This produces a very flat background. The isophotal detection process is then repeated. A Kron (1980)-type pseudo-total magnitude is then calculated for each image, using a local value of sky.

Table 1 shows the magnitude limits for our fields. As in our previous papers the minimum Kron radius is set to be that for an unresolved image of high signal-to-noise, and the correction to total is the light outside this minimum radius for such an image. Our measurement limits give the total magnitudes of unresolved objects which are a  $3\sigma$  detection inside the minimum radius (which is typically  $\sim 1.4''$  for the WHDF data). Star-galaxy separation was done on the  $B$  frame using the difference between the total magnitude and that inside a  $1''$  aperture, as described in Metcalfe et al. (1991). This enabled us to separate to  $B \sim 24^m$ . Some additional very red stars were identified from the  $R$  and  $I$  frames. As the WHDF is at high galactic latitude the stellar contamination should in any case be quite low. For the purposes of measuring the correlation function, masks files were also constructed to cover regions containing bright galaxies or stars. The area of the field affected by such bright objects is less than 10% of the total.

Similar methods were also used to generate catalogues from the north and south Hubble deep fields (i.e., we do not use any of the existing HDF catalogues but use our own independently written object detection and photometry software). One significant difference between the HDF data and our ground-based data is of course their much higher resolution. As described fully in Metcalfe et al (2000, in preparation), we visually inspect all detections on our HDF N/S data in an attempt to reduce the number of spurious entries in our catalogues. We also carry out a 'reassembly' process in which multiple detections on an individual galaxy are combined to produce a single detection. This admittedly subjective procedure is unavoidable in the HDF catalogues given the extremely high resolution of the data.

## 3 METHODS AND TECHNIQUES

### 3.1 Determining the angular correlation function

We use the normal estimator of Landy & Szalay (1993), given in equation 1. Here we follow the usual notation where  $DD$  indicates the number of galaxy-galaxy pairs,  $DR$  galaxy-random pairs and  $RR$  random-random pairs for a given angular separation and bin width:

$$\omega(\theta) = \frac{DD - 2DR + RR}{RR} \quad (1)$$

We find that, for a given survey sample, amplitudes measured by this estimator are very similar to those computed with the Hamilton (1993) estimator,  $\omega(\theta) = (DDRR/DR^2) - 1$ . The  $DD/DR - 1$  estimator, as used by Roche et al. (1993), gives consistently higher (at the 20–30% level) values for  $\omega(\theta)$ , over all our bins. This has been found by other authors and is indicative of the known biases inherent in this estimator (Hamilton 1993; Landy & Szalay 1993).

Filter	U	B	R	I	K	H
Limit ( $3\sigma$ )	26.8	27.9	26.3	23.5/25.6	20.0	22.5
Area (arcmin $^2$ )	48.5	48.5	48.5	88.3/53.0	47.2	50

**Table 1.** Photometric limits of the WHDF. The two magnitude limits in  $I$  refer to two separate surveys, one carried out at the INT (and covering 88.3 arcmin $^2$  and the other based on WHT data.

For a range of magnitude-limited samples of each catalogue,  $\omega(\theta)$  is computed using equation 1 for a series of bins spaced in increments of 0.2 in  $\log(\theta)$ , where  $\theta$  is in degrees. As we have only observed one field we cannot use the field-to-field variance to estimate the errors in each bin; instead we implement a bootstrap-resampling technique (Barrow, Sonoda, & Bhavsar 1984; Ling, Barrow, & Frenk 1986). In this method, the error in each bin is computed from the variance of the estimator as applied to a large ( $\sim 200$ ) number of bootstrap-resampled catalogues. As expected, these bootstrap errors are larger (normally  $\sim \times 2$ ) than the normal  $\sqrt{N}$  Poisson counting errors.

To allow comparison with other workers, we fit our measured correlations as a function of angular separation to an expression of the form

$$\omega(\theta) = A_\omega(\theta^{-\delta} - C) \quad (2)$$

where  $A_\omega$  is the amplitude of  $\omega(\theta)$  at  $1^\circ$  and  $C$  is the ‘‘integral constraint’’ term. This term is a bias which arises because we are using each catalogue to determine the mean galaxy density and is particularly significant in our work because the area which we survey is quite small. To calculate the integral constraint we use the expression

$$C = \frac{1}{\Omega^2} \int \int \theta^{-\delta} d\Omega_1 d\Omega_2 \quad (3)$$

where  $\theta$  is the angular separation of each galaxy pair and  $d\Omega_1$  and  $d\Omega_2$  the solid angle subtended by each pair. If we assume a power-law correlation function,  $\omega(\theta) \propto \theta^{-0.8}$  we may calculate this quantity for our fields by direct integration. Typically we find  $C \sim 13$  for the WHDF and  $\sim 40$  for the HDF (we must assume a slope for power-law correlation function as we cannot calculate it directly from this data;  $-0.8$  allows us to compare our work with similar studies in the literature).

The error on  $A_\omega$ , the overall fit, is determined from the method of Marquardt (1963), as described in Press et al. (1986). This method combines errors on each bin in an independent manner to calculate the total error of the fit. Figure 1 shows fits made for the  $B$ -band catalogue.

We determine correlation amplitudes for the Hubble deep field data using a similar procedure. In this case we fit our final power law to an average of the correlation function determined independently on each of the three WFPC2 chips. For our NICMOS correlation amplitude, we compute our correlation functions from the total numbers of pairs from both surveys. For all these space-based data sets the field of view is extremely small, and consequently the required integral constraint correction is very large. Additionally, the small numbers of pairs involved means that fits are generally dependent on three or fewer bins, and for this reason our resulting correlation amplitudes determined from these data should be regarded as upper limits on the fitted amplitudes, rather than definitive measurements. In order to

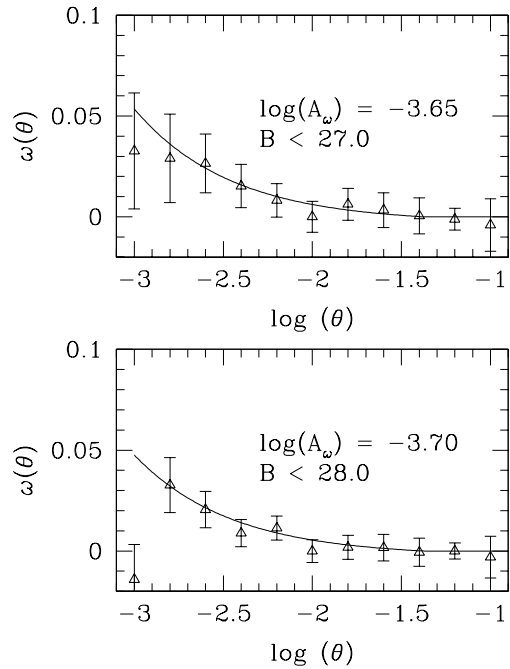


**Figure 1.**  $\omega(\theta)$  as measured for samples limited at  $B < 27^m$  and  $B < 28^m$ . The solid line shows the fit to  $\omega(\theta) = A_\omega(\theta^{-0.8} - C)$  where  $C$  is the ‘‘integral constraint’’ term described in the text and  $A_\omega$  is the value of  $\omega(\theta)$  at  $1^\circ$

try to reduce problems from ‘‘merged’’ objects as described in Section 2 we carry out our fits at angular separation  $> 1''$ .

### 3.2 Modelling the correlation function

We would like to compare our measured correlation amplitudes with those of model predictions. In order to do this we must assume a functional form for the spatial correlation function. From the results of large surveys (Groth & Peebles 1977; Davis & Peebles 1983; Maddox et al. 1990b) it is found that  $\xi(r)$  (the spatial correlation function) is well approximated by  $\xi(r) = (r_0/r)^\gamma$ , at least for scales  $< 20h^{-1}$  Mpc. Projecting a model for  $\xi(r)$  onto the two-dimensional distribution of galaxies measured by  $\omega(\theta)$  involves integrating this function over redshift space using Limber’s formula (Limber 1953).

We must parametrise the scaling of the correlation function with redshift. Early papers (Groth & Peebles 1977; Phillipps et al. 1978) assumed a scaling of the form

$$\xi(r, z) = h(z) \left( \frac{r_0}{r} \right)^\gamma \quad (4)$$

where

$$h(z) = (1+z)^{-(3+\epsilon)} \quad (5)$$

(in this case  $r$  is the proper distance); this relation has been used in many recent observationally-motivated studies investigating the projected two-point function (Efstathiou et al. 1991; Roche et al. 1993; Brainerd, Smail, & Mould 1994; Infante & Pritchett 1995a; Brainerd & Smail 1998).

To derive an expression for  $\omega(\theta)$ , the projected correlation function, we note that for small angles, the relation between  $\omega(\theta)$  and  $\xi(r)$  becomes (Efstathiou et al. 1991)

$$\omega(\theta) = \sqrt{\pi} \frac{\Gamma[(\gamma-1)/2]}{\Gamma(\gamma/2)} \frac{A}{\theta^{\gamma-1}} r_0^\gamma \quad (6)$$

where  $\Gamma$  is the incomplete gamma function,  $\theta$  is the angular separation and  $A$  is given by

$$A = \int_0^\infty g(z) \left( \frac{dN}{dz} \right)^2 dz / \left[ \int_0^\infty \left( \frac{dN}{dz} \right) dz \right]^2 \quad (7)$$

where

$$g(z) = \frac{h(z)}{d_A^{\gamma-1}(z) (dr(z)/dz)} \quad (8)$$

where  $d_A(z)$  is the angular diameter distance and  $dr(z)/dz$  is the derivative of the proper distance.

Analysis of the aforementioned large local redshift surveys suggests that  $\gamma = 1.8$ , leading to three cases of interest to us: clustering fixed in proper coordinates, in which case  $\epsilon = 0.0$ ; clustering fixed in co-moving coordinates which gives  $\epsilon = -1.2$ . Finally, the predictions of linear theory give  $\epsilon = 1.0$ . This formalism has been widely used in many papers which investigate the clustering of faint field galaxies: see, for example, Infante & Pritchett (1995b), Woods & Fahlman (1997).

As we have already noted, in these “epsilon models” characterised by equation 4 the co-moving galaxy correlation length decreases monotonically with redshift (providing of course  $\epsilon > -1.2$ , which produces models with clustering constant in co-moving co-ordinates) However, several recent works have indicated that this may not be a realistic assumption. In theoretical studies, both N-body simulations (Colin et al. 1999) and semi-analytic models (Baugh et al. 1999; Kauffmann et al. 1999) indicate that the co-moving galaxy correlation length decreases until  $z \sim 1 - 2$  after which it increases again. These theoretical studies (Governato et al. 1998) also allow us to explain the high clustering amplitudes observed for Lyman break galaxies at  $z \sim 3$  (Giavalisco et al. 1998; Adelberger et al. 1998) as a consequence of their formation in highly biased environments. Furthermore, the clustering growth is expected to be more rapid for less massive objects and for clustering amplitudes measured on smaller scales (Baugh et al. 1999).

Motivated by these works we also model our correlation amplitudes using a modification of equation 4. In place of the normal epsilon parametrisation, we have used in the relativistic Limber’s equation a more general form for the evolution of  $\xi(r, z)$ , namely

$$\xi(r, z) = \left( \frac{r_0^{\text{com}}(z)}{(1+z)r} \right)^\gamma \quad (9)$$

where  $r_0^{\text{com}}(z)$  is the comoving correlation length at  $z$ . Thus, we have used

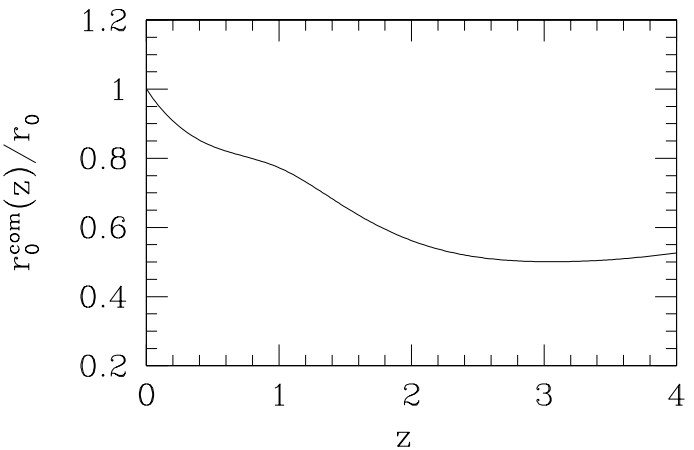


**Figure 2.** Normalised co-moving correlation length  $r_0^{\text{com}}(z)$  as fitted to haloes of circular velocity  $V > 120 \text{ km s}^{-1}$  as identified by Colin et al in the large N-body simulation of Kravtsov and Klypin (1999). This line is closest to the predictions of  $\epsilon = 0$  model described in the text.

$$h(z) = \left( \frac{r_0^{\text{com}}(z)}{(1+z)r_0} \right)^\gamma \quad (10)$$

To illustrate the possible effect of modelling more exactly the evolution of the correlation function, we have used the evolution seen in the large N-body simulation of Kravtsov & Klypin (1999); the semi-analytic models mentioned above produce a similar form for the evolution of  $\xi(r, z)$  in their simulations. As our field sample is dominated by spirals, we have therefore considered the haloes of the simulation having velocity  $v > 120 \text{ km s}^{-1}$ . Also, as  $\omega(\theta)$  for these deep fields has, as usual, been fitted to a  $-0.8$  power law, we have converted the Colin et al. data to provide the same correlation strength as a  $-1.8$  power law for  $\xi(r, z)$  at a comoving separation of  $0.3 h^{-1} \text{ Mpc}$ , which at the depths of our data here corresponds roughly to the angular scale of our estimates for  $\omega(\theta)$ . Finally, to obtain the function,  $r_0^{\text{com}}(z)$ , a spline fit was made to the converted Colin et al. data points with a simple linear extrapolation to redshifts larger than the maximum redshift,  $z = 5$ , for which they have estimated the correlation function for their simulation. Fig. 2 plots the resulting form of the evolution used for  $r_0^{\text{com}}(z)$  normalised to  $r_0$ . In using this in Limber’s equation, we have taken, as with Roche et al. (1993),  $r_0 = 4.3 h^{-1} \text{ Mpc}$ , which is little different from the converted Colin et al. value of  $4.2 h^{-1} \text{ Mpc}$ .

### 3.3 Calculating $dn/dz$

From equation 7 we see that the amplitude of  $\omega(\theta)$  depends on the redshift distribution,  $dn/dz$ . To produce these redshift distributions we employ a pure luminosity evolution (PLE) model in which star-formation increases exponentially with look-back time. Earlier versions of these models are discussed in our previous papers (Metcalfe et al. 1991; Metcalfe et al. 1995; Metcalfe et al. 1996), and a full description of the model used in this paper is given in (McCracken et al. 2000). In this paper we assume  $H_0 = 50 \text{ kms}^{-1} \text{Mpc}^{-1}$ , although changing the value of  $H_0$  does not markedly affect our conclusions. Two values of the deceleration parameter  $q_0 = 0.05$  and  $q_0 = 0.5$ , are adopted, corresponding to open and flat cosmologies respectively. The input parameters to our models consist of observed *local* galaxy parameters (namely, rest-frame colours and luminosity functions) for each of the five morphological types (E/S0, Sab, Sbc, Scd and Sdm) we consider in our models. These morphological types are divided into early-type (E/S0/Sab) and spiral (Sbc/Scd/Sdm) and these two classes are each given a separate star-formation history, parametrised in terms of an e-folding time  $\tau$ . We compute the  $k + e$  corrections using the models of Bruzual & Charlot (1993). We could, in principle, sub-divide the spirals into different morphological types each with different star formation histories but for simplicity we do not; ( $k + e$ ) corrections for the different types are fairly similar to each other in these models in any case. Instead, taking a Sbc model as representative of all types we produce the other types by normalising the Sbc track to the observed rest-frame colours. As in our earlier papers (Jones et al. 1991; Metcalfe et al. 1991; Metcalfe et al. 1995; McCracken et al. 2000), the normalisations of our luminosity functions are chosen to match the galaxy counts at  $B \sim 18 - 20$  and we seek to explain the low number counts at bright magnitudes from a combination of photometric errors and anomalous galaxy clustering, rather than substantial and hence unphysical evolution at low redshift in the luminosity of galaxies. Our models also include the effects of the Lyman- $\alpha$  forest, and, for spiral types, dust extinction corresponding to the Large Magellanic Cloud as described in Pei (1992). The model redshift distributions produced are in good agreement with the redshift distributions of the CFRS (Lilly et al. 1995a) and from the Keck Hawaii redshift survey (Cowie, Songaila, & Hu 1996). To illustrate the effect which the inclusion of the evolutionary corrections have on our computed correlation function scaling relation, we also calculate an non-evolving redshift distribution. This is produced by applying  $k -$  corrections only to each galaxy type.

## 4 MEASURED AMPLITUDES

In this Section we will present a comparison between our measurements of  $A_\omega$  and those in the literature. We defer an analysis of the implications these measurements have for the growth of galaxy clustering, as well as a discussion of our evolutionary models, to Section 5; here we present comparisons only with the non-evolving,  $\epsilon = 0$ ,  $q_0 = 0.05$  model.

In panels a–d of Figure 3 we plot our fitted correlation amplitudes extrapolated to one degree (filled symbols, circles for WHDF and squares for HDF) as a function of sample limiting magnitude for *BRIK* bandpasses in comparison

with measurements from the literature (open symbols). The solid line shows the predictions of the stable clustering,  $\epsilon = 0$  non-evolving (i.e., no luminosity evolution) model, computed assuming  $r_0 = 4.3h^{-1}$  Mpc and  $q_0 = 0.05$  (This value of  $r_0$  was chosen to produce the correct clustering amplitude at brighter magnitudes as measured from early Schmidt plate surveys (Jones, Shanks, & Fong 1987; Stevenson et al. 1985). We adopt the same value of  $r_0$  for all bandpasses; in Section 5.4 we discuss if this is an appropriate assumption for our data.)

Starting with the  $B -$  band, we note that here our WHDF sample reaches extremely high galaxy surface density—approaching  $\sim 10^6 \text{ gal deg}^{-2}$  at  $B = 28^m$ , and furthermore it probes to the highest redshift; our low- $q_0$  evolutionary models indicate that by  $B \sim 28$  we reaching  $z_{med} \sim 2$ . Moreover, our measurements of the  $B -$  band correlation function are significantly deeper than any previously published work. Our brightest bin, at  $B < 27.0$ , is in agreement with the correlation amplitude measured by Metcalfe et al. (1995). Faintwards of  $B = 27$ , our correlation amplitudes remain flat. The errors on our fitted correlations in  $B$  are relatively low in comparison with our other bandpasses because at  $B < 28$  we detect  $\sim 6000$  galaxies, more than in any other bandpass. Our HDF-N/S clustering measurements are in agreement with the measurement from the much larger area of the WHDF.

Our non-evolving models have some important differences with those used in the earlier works of Roche et al. (1993) and Metcalfe et al. (1995). Firstly, our models include the effects of internal extinction by dust (corresponding to  $A_B = 0.3$  mag, using the dust model of Pei (1992)) and reddening by the Lyman alpha forest (as modelled in Madau (1995)). Both of these effects may become significant at the very faintest magnitudes we reach, where  $z_{med} > 2$ . Secondly, our  $k -$  corrections are computed from the models of Bruzual & Charlot (1993) for both our evolving and non-evolving models, whereas Roche et al. (1993) and Metcalfe, Fong, & Shanks (1995) used polynomial fits to the spectral energy distributions of Pence (1976) for their non-evolving models. These fits extend only to  $z \sim 2$  and are held constant at higher redshifts. Thirdly, the redshift distributions in these earlier papers were artificially truncated at  $z = 3$ . The sum effect of these differences is that in Roche et al. (1993) and Metcalfe et al. (1995) the slope of the  $A_\omega -$  magnitude limit scaling relation remains constant whilst our slope begins to decrease at  $B \sim 26$ . By this magnitude limit the difference between our predictions and these previous works is  $\sim 0.2$  in  $\log(A_\omega)$ .

Our  $R -$  band correlations plotted in panel (b) of Figure 3 reach  $R < 26$ , although the number of galaxies in this catalogue is much smaller ( $\sim 300$ ) than in  $B -$  and consequently our errors are larger. Our measured clustering amplitude at  $R < 25.5$  agrees well with the faintest data point of Brainerd, Smail, & Mould (1994); unfortunately, our survey area is too small to permit us to check our clustering amplitudes with values from the literature measured at brighter magnitudes such as the large,  $\sim 2 \text{ deg}^2$  CCD survey of Roche & Eales (1999). Our measured clustering amplitudes in  $R -$  in the WHDF are *much lower* than the predictions of the non-evolving, stable clustering model. Our HDF clustering measurements are in good agreement with

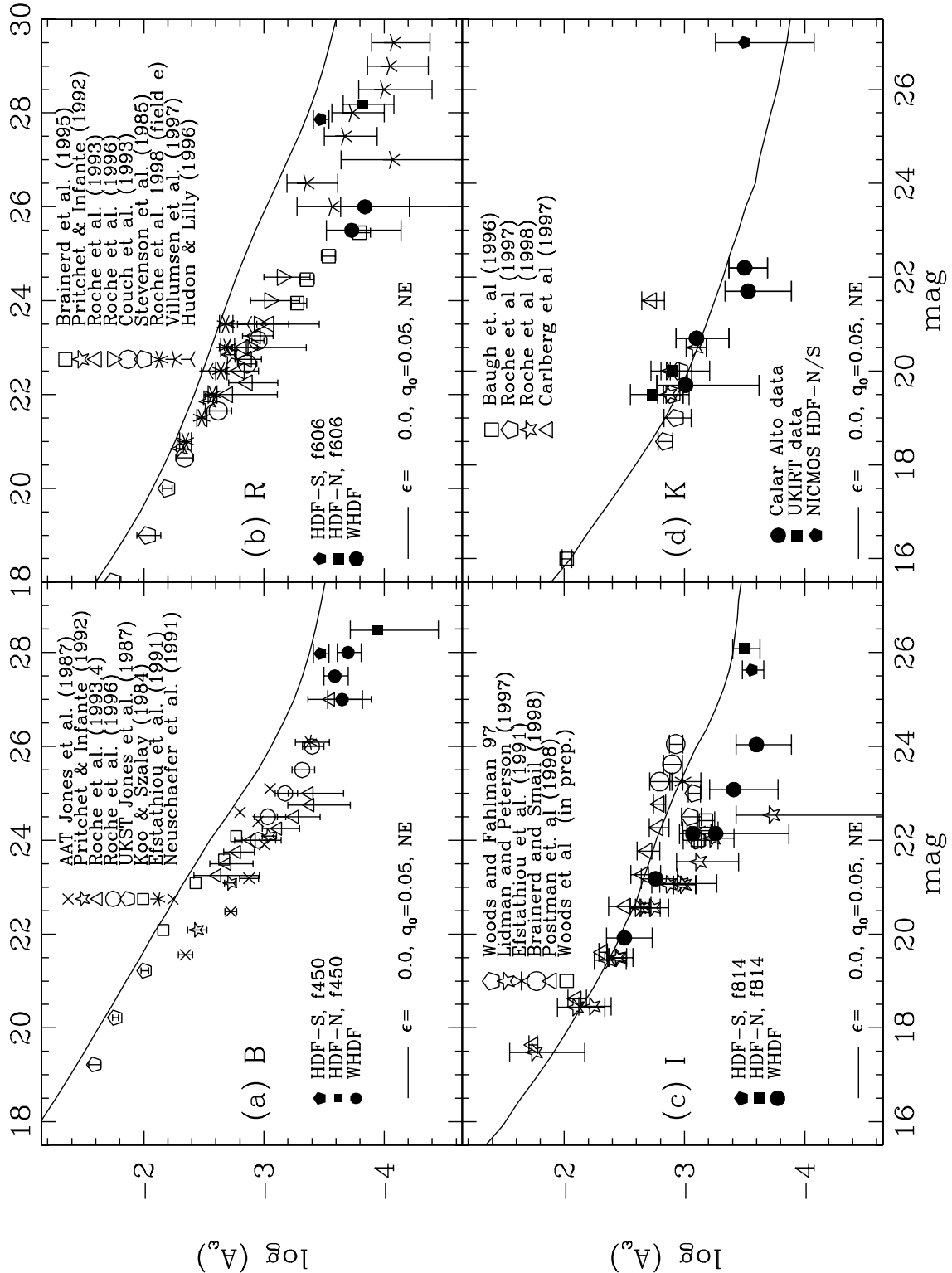


**Figure 3.** The logarithm of the amplitude of the angular correlation function  $\omega(\theta)$  at one degree ( $A_\omega$ ) in the WHDF (filled circles), HDF-N (filled squares) and HDF-S (filled pentagons) shown as a function of apparent magnitude for BRIK selected samples (panels a-d). For  $I$ , correlations are plotted as a function of sample median magnitude. Open symbols show points from the literature. The solid line shows the predictions a non-evolving model with  $\epsilon = 0$  and with  $r_0 = 4.3 h^{-1} \text{ Mpc}$  and  $q_0 = 0.05$ . Error bars on our measurements are calculated by a bootstrap resampling technique, as described in Section 3.1 .

the HDF clustering measurements of Villumsen, Freudling, & Da Costa (1997).

For our  $I$ -band measurements, shown in panel (c) of Figure 3, we follow the practice in the literature and show correlation amplitudes as a function of sample *median* magnitudes and not limiting magnitudes. We follow the same procedure for our model correlation amplitudes which are plotted at the median magnitude of each magnitude limited slice. In addition to our  $I < 26$  WHT data, we have a second, larger image taken at the INT which overlaps the WHDF. This covers a total of  $\sim 80$  arcmin $^2$  to  $I < 23.5$  and allows us to determine  $A_\omega$  from  $I_{med} = 20$  to  $I_{med} = 22$  (the three brightest WHDF bins on the graph). The faintest bin in this INT dataset is in agreement with our measurements from the brightest bin of the WHT dataset. Furthermore, the preliminary result from the large-area 0.2 deg $^2$  survey of Woods et al. (in preparation), shown as an open square, is in agreement with our WHT measurement. At  $I_{med} \sim 26$ , measurement from the HDF fields appear to favour the lower values found in the WHDF. We note also that fainter  $I_{med} \sim 21$ , our measurement are below the predictions of the non-evolving  $\epsilon = 0$  model.

Faintwards of  $I_{med} \sim 23$  a discrepancy emerges between our measurements and two previously published studies. At  $I_{med} \sim 24$ , our WHDF clustering measurements are  $\sim 5$  times lower than the measurements made by Brainerd & Smail (1998) over two slightly smaller fields of area  $\sim 30$  arcmin $^2$  at a similar limiting magnitude. At brighter magnitudes, our points are also below the faintest bins of Postman et al. (1998). This work is a large-area CCD survey covering a contiguous 16 deg $^2$  area and is currently the most reliable determination of galaxy clustering over wide angles and at intermediate ( $z \sim 1$ ) depths. We defer a detailed analysis of these differences until Section 4.1 where we will attempt to quantify if the discrepancies between our survey and the works of Postman et al. and Brainerd & Smail could be explained in terms of cosmic variance effects.

Finally, we turn to an investigation of galaxy correlations for  $K$ -selected samples. Until very recently measuring  $\omega(\theta)$  at near-infrared wavelengths was time-consuming and difficult as typical detectors covered only  $\sim 1$  arcmin $^2$ . However, wide-format IR arrays are becoming available making it now possible to conduct wide, deep surveys of the near-infrared sky. The filled circles in panel (d) of Figure 3 shows clustering amplitudes determined from our faint,  $H < 22.5$ , wide area ( $\sim 50$  arcmin $^2$ ) Calar Alto Survey are shown, which will be described fully in a forthcoming paper (McCracken et al. 2000, in preparation). Similarly, also plotted are clustering measurements from our  $6' \times 6'$  UKIRT IR-CAM3 mosaic (McCracken et al. 2000). At  $K \sim 27$  we have computed a single point from NICMOS data taken as part of the north and south Hubble deep fields program (we transform from  $H$  to  $K$  using a model  $(H - K)$  colour). We note that all our measurements are in agreement with the predictions of our stable clustering, no luminosity evolution model.

In plotting the  $H$ -limited Calar Alto points on our  $K$ -limited scaling relation we make two assumptions: firstly, at  $K \sim 22$ ,  $(H - K) \sim 0.3$ ; and secondly, for a given surface density, the clustering properties of  $H$ -selected and  $K$ -selected galaxies is identical. The first assumption seems reasonable, given that at  $K \sim 20$ , galaxies in our survey have  $(H - K) \sim 0.3$  and it is unlikely that they become signifi-

cantly bluer by  $K \sim 22$ . The  $K$ -selected ( $I - K$ ) histograms shown in McCracken et al. (2000) support this. Also given that our Calar Alto  $H < 20$   $A_\omega$  agrees with our UKIRT  $K < 19.5$  point, we conclude that our second assumption is also valid.

Our points at  $K = 19 - 20$  agree with the survey of Roche, Eales, & Hippelein (1998) and Roche & Eales (1999); however at fainter magnitudes there is a discrepancy between our amplitudes and the measurement of Carlberg et al. (1997). Once again, we defer a detailed discussion of the possible explanation of these differences until the following section.

#### 4.1 Quantifying errors in the correlation function

In this Section we will investigate if we have estimated the magnitude of our correlation function error bars correctly. The small size of our field means our integral constraint (equation (3) corrections are large, and consequently accurate measurements of  $\omega(\theta)$  are dependent on an accurate determination of this quantity. Our main motivation is to see if we can explain the discrepancies between our measurements of  $A_\omega$  at  $I < 25$  and  $K \sim 21.5$  with those of Brainerd & Smail (1998) and Carlberg et al. (1997). There are already indications that such “extra” variance could be significant at the depths of our survey. Postman et al. (1998) directly address this question at shallower depths in their work which covers  $\sim 16$  deg $^2$ . By extracting 250 independent  $16' \times 16'$  fields from their survey (each of which is five times larger than the WHDF but at a brighter limiting magnitude) they find that the variance on  $\omega(1')$  is comparable to its mean value of  $\sim 0.045$ , with extreme values reaching  $\times 3$  this. Furthermore, they suggest that as the error distribution for  $A_\omega$  is non-Gaussian, and skewed positively, there could be many more areas in which  $A_\omega$  is below the mean value, rather than above it.

To quantify the amount of “extra” variance which could affect clustering measurements in a very deep field like the WHDF we adopt a simple approach and generate large mock catalogues using the method of Soneira & Peebles (1978). This is an purely empirical approach to generate a hierarchically clustered distribution of points. We start by placing within a sphere of radius  $R$  a random distribution of sub-spheres each of radius  $R/\lambda$ . Within each of these a further  $n$  spheres of radius  $R\lambda^2$  are added. This continues through  $L$  levels; in our simulation we adopt  $L = 9$ . The amplitude of the correlation function is fixed by the number of centres used and the fraction of the total number of points which are retained; these quantities must be determined by trial and error.

We measure the variance on the correlation function for many subsamples of this catalogue. We start by generating a catalogue covering 6.25 deg $^2$  with the same surface density of objects as in our real catalogue at  $I < 25$  (corresponding to  $\sim 7.5 \times 10^5$  galaxies). Next, we measure  $\omega(\theta)$  over the full simulated catalogue area. Our aim is to produce a catalogue for which the fitted correlation amplitude  $\log(A_\omega)$  at  $I < 25$  is midway between the result of Brainerd & Smail ( $\log(A_\omega) = -2.93^{+0.05}_{-0.06}$ ) and our own ( $\log(A_\omega) = -3.61^{+0.16}_{-0.26}$ ). Once a catalogue with the desired correlation amplitude is produced it is randomly subsampled to produce 200 sub-areas each of which has the

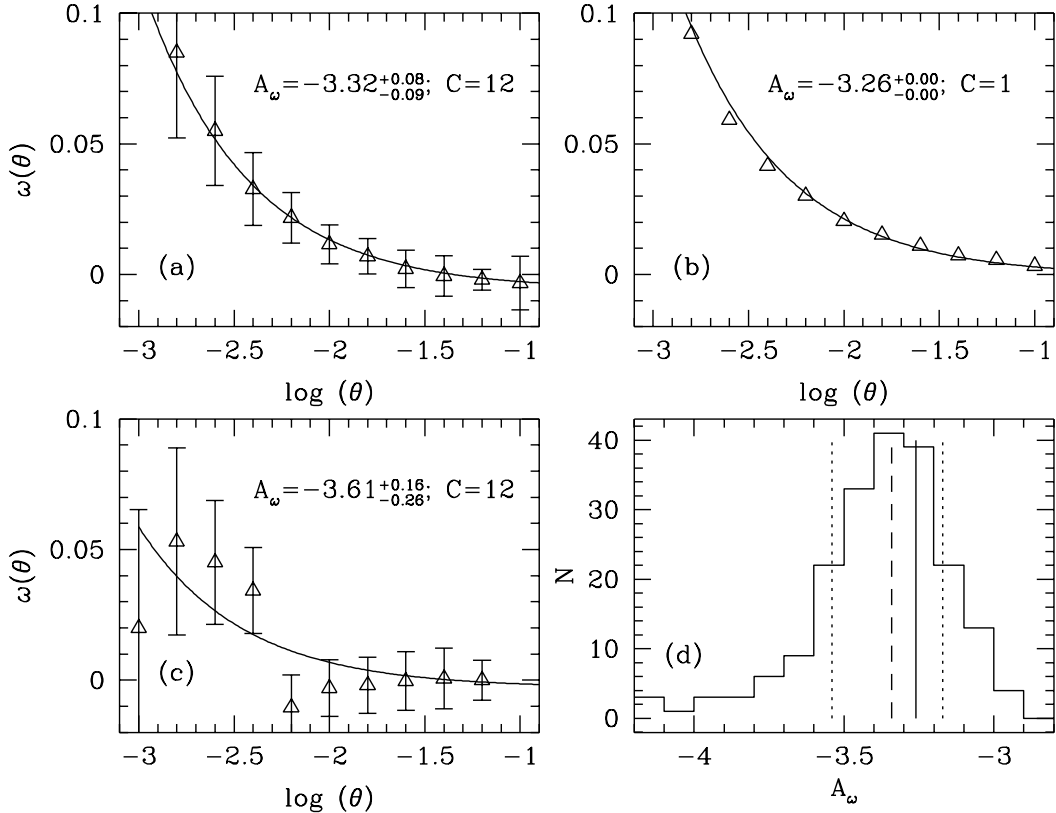


**Figure 4.** Results from simulations of a  $6.25 \text{ deg}^2$  area with the same surface density of objects as our  $I < 25$  catalogue. Panel (a) shows  $\omega(\theta)$  measured from an average of two hundred sub-areas each covering  $50 \text{ arcmin}^2$  (corresponding to the size of the WHDF), with error bars calculated using the normal bootstrap-resampling technique; panel (b) shows  $\omega(\theta)$  determined from the full simulation. Panels (c) and (d) show  $\omega(\theta)$  as measured at  $I < 25$  from the WHDF (again with error bars calculated using bootstrap-resampling) and the histogram of fitted values for  $\log(A_\omega)$  from the simulations. The dotted lines shown on the histogram represent  $\pm 1\sigma$  deviations from the median value; the full simulation value is shown as the solid line and the average value as the dashed line. From this histogram we determine  $\log(A_\omega) = -3.35^{+0.18}_{-0.17}$ .

same field of view ( $\sim 50 \text{ arcmin}^2$ ) and galaxy surface density at  $I \sim 25$  as the WHDF (this translates to  $\sim 2000$  objects per field). On each of these sub-fields correlation amplitudes are measured using the same parameters as for the real data set, and a histogram is computed using each of these individual measurements of the simulated data.

Figure 4 presents results from one set of simulations. Panel (b) in this Figure shows the measured correlation function for a synthetic catalogue generated using the method outlined above (error bars have not been plotted as they are smaller than the symbols for all bins). For this catalogue we find  $\log(A_\omega) = -3.26$  for an integral constraint  $C = 1$ . Panel (a) shows the average value of  $\omega(\theta)$  from two hundred sub-samples of this catalogue, as well as the fitted value to this average which we find to be  $\log(A_\omega) = -3.32^{+0.08}_{-0.09}$ . For comparison, the fit to our  $I < 25$  observations is shown in panel (c); for the real data we find  $\log(A_\omega) = -3.61^{+0.16}_{-0.26}$ .

This procedure tests several important aspects of our technique. Because our simulated field is so large, the integral constraint correction (Equation 3) which must be applied to it is much smaller than the amount required for each of the individual sub-fields. Given that the  $A_\omega$  which we measure from the full survey agrees to within the fitting errors to the  $A_\omega$  determined from the average of two-hundred sub-fields we conclude that errors arising from an incorrect determination of the integral constraint are not significant. However, the agreement between the sub-fields and full-survey values is perhaps not surprising as both the catalogue and  $C$  were generated and calculated assuming a power-law slope  $\delta$  for  $\omega(\theta)$  of  $-0.8$ . There is some indication that  $\delta$  becomes flatter at fainter magnitudes (Postman et al. 1998) although we are unable to test this with our current data set. A flatter correlation function at fainter magnitudes would lead to an underestimate of the integral constraint and a consequent underestimate of  $A_\omega$ .

More significantly for this current work, however, is the large dispersion we find for the fitted  $A_\omega$ 's from our simulated fields. Panel (d) of Figure 4 illustrates this. From this diagram,  $\log(A_\omega) = -3.35^{+0.18}_{-0.17}$  ( $1\sigma$  errors). This corresponds to a linear error of  $\pm 2.2 \times 10^{-4}$ . By comparison, our errors determined from our bootstrap resamplings are  $\pm 1.1 \times 10^{-4}$ ; Brainerd & Smail's errors are  $\pm 1.5 \times 10^{-4}$ . Their points are an average of two widely separated  $\sim 30$  arcmin $^2$  fields and at  $I < 25$  contain approximately the same numbers of galaxies as our catalogue. On the basis of these simulations we conclude both our errors and those of Brainerd & Smail underestimate the true error. Additional simulations at higher amplitudes also have higher variances; a second simulation at  $\log(A_\omega) = -3.1$  has a  $1\sigma$  error of  $\pm 2.6 \pm 10^{-4}$ . Adopting errors of this size, we find that our correlation measurement is consistent with that of Brainerd & Smail at the  $2.5\sigma$  level.

Turning to the  $K$ -selected correlation amplitudes plotted in Figure 3 we note that at  $K < 21.5$  over  $\sim 27$  arcmin $^2$  Carlberg et al. (1997) measure  $\log(A_\omega) = -2.72^{+0.08}_{-0.10}$ . This is also different from our work: at  $K < 21.7$  we measure  $\log(A_\omega) = -3.53^{+0.19}_{-0.36}$  in an area of  $\sim 44$  arcmin $^2$ . The number density of galaxies at  $K \sim 21$  is approximately the same as at  $I \sim 25$ , and the amplitude of Carlberg et al.'s point is also within  $\sim 40\%$  of Brainerd & Smail's point. Moreover, as we have described above, we find a larger variance on  $\omega(\theta)$  for simulations of higher amplitude. These considerations leads us to conclude that the stated error bar on Carlberg et al.'s measurement is also an underestimate of the true error. Furthermore, we conclude that our "low" results at  $I \sim 25$  and  $K \sim 21$  are *not* inconsistent with the other results in the literature, given the large error bars afflicting measurements of  $A_\omega$  in fields of this size and at these depths.

## 5 INTERPRETATION AND DISCUSSION

### 5.1 Galaxy clustering models

After a decade of study, the general characteristics of galaxy evolution in the range  $z = 0 - 1$  have been broadly outlined, although many specific details have yet to be worked out, such as parameter dependence on morphology and intrinsic luminosity. Galaxy samples selected in bluer bandpasses are dominated by starburst populations as has been confirmed by many spectroscopic surveys (Lilly, Cowie, & Gardner 1991; Glazebrook et al. 1995; Cowie, Songaila, & Hu 1996), whereas samples selected in redder bandpasses show median redshifts and number count distributions which are closer to the non-evolving predictions (Metcalfe et al. 1996; Cowie, Songaila, & Hu 1996). This mirrors broad trends seen in studies of the evolution of luminosity functions of colour-selected galaxy samples (Lilly et al. 1995b; Ellis et al. 1996; Lin et al. 1997; Lin et al. 1999), although distinguishing between density and luminosity evolution in these surveys is not straightforward. In interpreting our observations in terms of luminosity evolution models we are well aware of the limitations of these class of models, such as the difficulty in correctly reproducing the properties of near-infrared selected samples. Instead, we present our models as a simple parametrisation of the observations using a model motivated by the star-formation behaviour of the entire galaxy

population. As shown in Metcalfe et al. (2000), the integrated star-formation history implied by our models agrees with current estimates of the global star-formation history of the Universe. The agreement between our predicted redshift distributions and observations at brighter magnitudes (Metcalfe et al. 1996; McCracken et al. 2000) gives us confidence in using these models to investigate the growth of galaxy clustering.

In panels a-d of Figure 5 we plot our measurement of  $A_\omega$  for *BRIK* bandpasses (filled symbols) in comparison with the literature (open symbols), in addition to the predictions of our evolutionary models with  $\epsilon = -1.2, 0, 1.0$ . We also consider a model with zero spatial curvature and a non-monotonic  $r_0 - z$  relation, as explained in Section 3.2. In comparing these four graphs, it is interesting to notice how the *shape* of the scaling relation is qualitatively different from bandpass to bandpass. To understand the origin of these differences, we start by emphasising that *amplitude* of the correlation function is directly related to the sample median redshift. From Eq. (4) we see that  $A_\omega$  depends on the width of the redshift distribution, as well as its median value. Our model scaling relations are therefore indicative of the median redshift of the model population. Other workers have commented on this relation previously (Koo & Szalay 1984); in this section we will attempt to see if our two-population luminosity evolution model can be used to explain the differences between the observed scaling of the correlation function amplitudes.

Starting with the  $B$ -band scaling relation, we note that in this bandpass in all magnitude slices, the model population is dominated by spiral galaxies. Brighter than  $B \sim 22$ , evolutionary effects are negligible; however, faintwards of this, galaxies undergo 1–2 magnitudes of brightening, and a significant high-redshift tail becomes evident. For this reason the slope of the  $B$ -band number counts is steepest in this range. The effect of this evolutionary brightening is to cause the median redshift of the  $B$ -selected redshift distributions to increase rapidly faintwards of  $B \sim 24$ ; at  $B \sim 22$ ,  $z_{med} \sim 0.3$ , but by  $B \sim 24$ ,  $z_{med} \sim 0.7$  and by  $B \sim 25$ ,  $z_{med} \sim 1$ . This causes  $A_\omega$  to drop rapidly below the non-evolving prediction. This extended  $B$ -band redshift distribution, confirmed in the spectroscopic survey of Cowie, Songaila, & Hu (1996), allows us to explain the observed clustering amplitudes without recourse to positing a hypothetical, weakly clustered population dominating the  $B$ -selected samples, as did some earlier authors (Brainerd, Smail, & Mould 1994; Infante & Pritchett 1995a). In redder bandpasses, the situation is slightly different; for example, in  $R$  spiral evolution is more gradual than in  $B$ , causing a much less pronounced slope change in the  $A_\omega$ -magnitude relation at  $R \sim 24$ . Similar considerations apply to the  $I$ -band. By the  $K$ -band, however, the form of the  $A_\omega$  limiting magnitude relation is determined primarily by the early-type population; although the early-type counts turn over at  $K \sim 20$  they still comprise more than half of the total galaxy population faintwards of this. Consequently, the  $A_\omega$ -limiting magnitude relation has constant slope as these galaxy samples are dominated by slowly-evolving early-type populations.

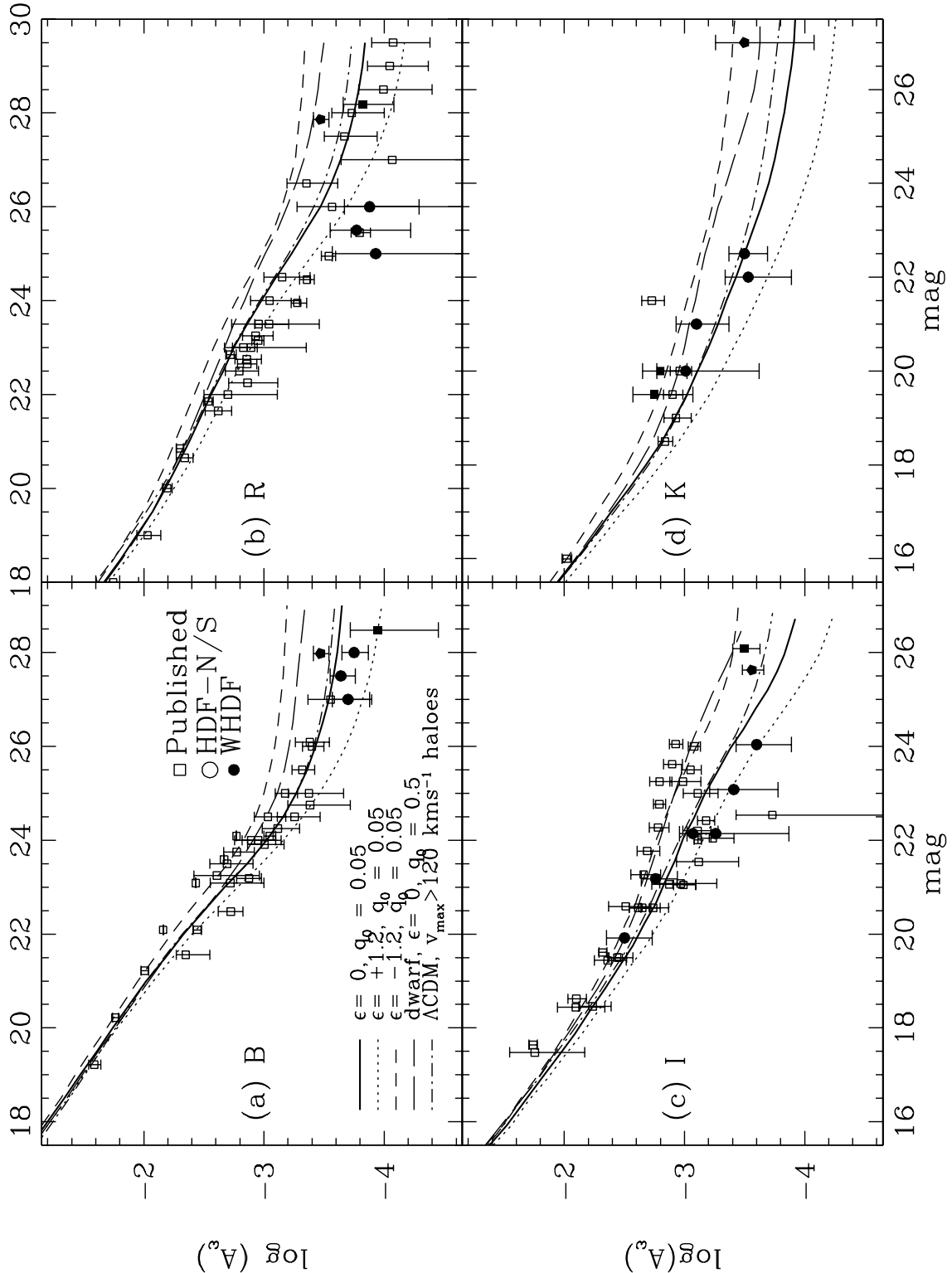


**Figure 5.** The logarithm of the amplitude of the angular correlation function  $\omega(\theta)$  at one degree ( $A_\omega$ ) in the WHDF (filled circles), HDF-N (filled squares) and HDF-S (filled pentagons) shown as a function of apparent magnitude for *BRIK* selected samples (panels a–d). For *I*, correlations are plotted as a function of sample median magnitude; open symbols show points from the literature. Error bars on our measurements are calculated by a bootstrap resampling technique as described in Section 3.1. Also shown are the predictions of our best-fitting evolutionary model for three values of the clustering growth parameter  $\epsilon$  and for  $r_0 = 4.3h^{-1}$  Mpc and  $q_0 = 0.05$ . The long dashed line shows the predictions of the  $\epsilon = 0$ ,  $q_0 = 0.5$  dwarf-dominated model, and the dot-dashed line shows the predictions for the  $\Omega_\Lambda = 0.7$  case with dynamical evolution for haloes with rotation velocities  $> 120 \text{ km s}^{-1}$ .

## 5.2 Model comparison with observations

From a visual inspection of Figure 5, our low- $q_0$  evolutionary model with  $\epsilon = 0 - 1$  provides the best fit to the data at all magnitude limits; in the following Section we will present a quantitative analysis of the growth of clustering implied by our models.

At fainter magnitudes, certain models are disfavoured; for example, the  $q_0 = 0.5$ , dwarf-dominated model, shown in Figure 5 as the long dashed line, produces much higher correlation amplitudes than the observations fainter than  $B \sim 26$ . This is because, in general, the median redshift of a magnitude-limited sample is lower for a low- $q_0$  cosmology than for a high- $q_0$  one, because the differential volume element is smaller in the latter case. Consequently, for the same value of  $\epsilon$  and  $r_0$ ,  $A_\omega$  is higher for  $q_0 = 0.5$  than it is for  $q_0 = 0.05$ . For this reason, our  $\epsilon = 0$ ,  $q_0 = 0.5$  dwarf model predicts higher clustering amplitudes than our standard  $\epsilon = 0$ ,  $q_0 = 0.05$  model. The exact magnitude of the differences between the two models depends (in addition to the cosmological considerations outlined above) on where the median redshift of galaxies in the high- $q_0$  model is greater than unity, where the star-formation rate for the dwarf types is constant, or less than unity, and where they rapidly fade. This high clustering amplitude leads us to reject the dwarf-dominated,  $\epsilon = 0$ ,  $q_0 = 0.5$  model. Of course, this conclusion is dependent on the dwarf population having the same intrinsic clustering properties as the normal galaxy population, which may not be the case (Roche et al. 1993; Infante & Pritchett 1995a).

Earlier works conducted in  $B$ -selected surveys suggest that by  $B \sim 26$ ,  $A_\omega$  ceases to decline and reaches a constant, limiting value (Roche et al. 1996; Metcalfe et al. 1995; Roche et al. 1993); more recently, Brainerd & Smail (1998) claimed to have detected a similar phenomenon at  $I_{med} \sim 24$ . The scaling relation for our  $B$ -band evolutionary model, shown in Figure 5, flattens off at very high number densities ( $\log(N_{gal}) \sim 6 \text{ deg}^{-2}$ ) and faint magnitudes ( $B \sim 28$ ). At these limits, the relationship between number density and median redshift levels off. This is a consequence of the steep faint-end slope luminosity function assumed for Scd and Sdm spiral galaxies (which have Schechter (1976) function parameter  $\alpha = -1.5$ ), which means that at fainter magnitudes one observes intrinsically fainter rather than more distant galaxies, and also of the reduction of the cosmological volume element at high redshift. Our  $B$ -band correlations reach depths at which the correlation function is expected to behave in this manner, and indeed from  $B = 27.0$  to  $B = 28.0$  we do observe that the amplitude of  $A_\omega$  is almost independent of magnitude.

What are the implications of our  $K$ -selected  $A_\omega$  measurements? In McCracken et al. (2000) we demonstrated how the low median redshift found for  $K$ -selected redshift distributions (Cowie, Songaila, & Hu 1996) placed stringent limits on the amount of evolution allowable in these bandpasses. In order for our PLE models to fit Cowie, Songaila, & Hu's  $K < 19$  redshift distribution (which has a very low median redshift, close to the predictions of a non-evolving model), we had to assume a steep slope ( $x = 3$ ) for the initial mass function. This reduces the amount of passive evolution at  $K$ -for early-types, resulting in a total galaxy population with a lower median redshift (Figure 5 of McCracken et al.

(2000), illustrated how the variations in IMF slope could affect the redshift distributions).

As we can see from Figure 5 our  $\epsilon = 0$ , low  $q_0$  evolutionary model incorporating this steep IMF slope fits the observed clustering amplitudes for  $K$ -selected samples quite well. Therefore, the observed clustering amplitudes are consistent with the underlying redshift distribution for  $K$ -selected samples which has a low median redshift, close to the predictions of the non-evolving model. More significantly—and beyond the spectroscopic limit of the even the Keck telescope—our Calar Alto data at  $H \sim 22$  indicates that even at these very faint magnitude levels, the  $H$ -selected galaxy correlations are *still* consistent with the non-evolving prediction. Galaxy merging, however, could provide another explanation for the low median redshift we infer for our  $K$ -sample. A low median redshift for  $K$ -selected surveys is a general prediction of the models of hierarchical galaxy formation (Kauffmann & Charlot 1998).

## 5.3 Measuring the rate of clustering evolution

In this Section we investigate what implications our measurements  $A_\omega$  have for the growth of galaxy clustering. As we have commented earlier, the small angular size of the WHDF means we are probing very small scales where the growth of galaxy clustering is expected to be highly non-linear. Most of the power in our correlation function signal comes from our inner bins, at angular scales of  $\sim 0.2'$ ; at  $z \sim 1$ , the typical median redshift of our samples, this translates to linear dimensions of  $\sim 0.05h^{-1} \text{ Mpc}$  (for  $q_0 = 0.05$ ). Additionally, how our samples are selected will affect clustering amplitudes. In our flux-limited catalogues, a range of galaxy luminosities will be present, and local redshift surveys have shown that clustering amplitude may be a function of luminosity and morphology (Loveday et al. 1995; Tucker et al. 1997).

With these caveats in mind, in Table 5.1 we present the results for best-fitting values for the parameters  $r_0$  and  $\epsilon$  in Equation (1) determined by  $\chi^2$  minimisation using our WHDF observations and the model ( $\Lambda = 0$ ,  $q_0 = 0.05$ ) outlined in Section 3.2. As before, we use redshift distributions determined from our best-fitting evolutionary model. Because of the strong co-variance between  $r_0$  and  $\epsilon$  it is not possible to derive both parameters simultaneously from our dataset; instead we investigate what values of  $r_0$  and  $\epsilon$  are implied by “reasonable” choices of these parameters.

We wish to investigate what value of  $\epsilon$  best fits our data and to do this we fix  $r_0$  to  $4.3h^{-1} \text{ Mpc}$ . This value of  $r_0$  is chosen to agree with angular correlation measurements determined from large Schmidt plate surveys. More recent work from local redshift surveys approximately agrees with this value. For example, Loveday et al. (1995) find for the  $b_J$  selected APM an  $r_0$  of  $5.1 \pm 0.2h^{-1} \text{ Mpc}$  and  $\gamma = 1.71$ . The  $R$ -selected Las Campanas Redshift Survey (Tucker et al. 1997) finds  $r_0 = 5.0 \pm 0.14h^{-1} \text{ Mpc}$ .

In general, we find  $\epsilon \sim 0$  for  $r_0 = 4.3h^{-1} \text{ Mpc}$  and  $q_0 = 0.05$ , from our own data alone. As we have already discussed, in the  $I$ -band our points are different from those of Brainerd & Smail at the  $\sim 3\sigma$  level. Their survey subtends  $\sim 30'$  on the sky, and reaches similar depths to our own work, and so we would expect this survey to sample the same environments as our own, and therefore to show broadly

Bandpass	$\epsilon$ ( $r_0 = 4.3 h^{-1}$ Mpc)	$r_0$ ( $\epsilon = 0$ )
<i>B</i>	$0.40^{+0.35}_{-0.30}$	$3.70^{+0.45}_{-0.50}$
<i>R</i>	$2.65^{+1.30}_{-0.65}$	$2.30^{+0.75}_{-1.05}$
<i>I</i>	$1.10^{+0.75}_{-0.50}$	$3.35^{+0.45}_{-0.45}$
<i>K</i>	$0.05^{+0.65}_{-0.45}$	$4.30^{+0.70}_{-0.80}$

**Table 2.** Best-fit values for  $\epsilon$  for  $r_0 = 4.3 h^{-1}$  Mpc and for  $r_0$  for  $\epsilon = 0$ , using redshift distributions computed from our best-fitting evolutionary model and assuming  $q_0 = 0.05$ . Errors quoted are  $\pm 1\sigma$ .

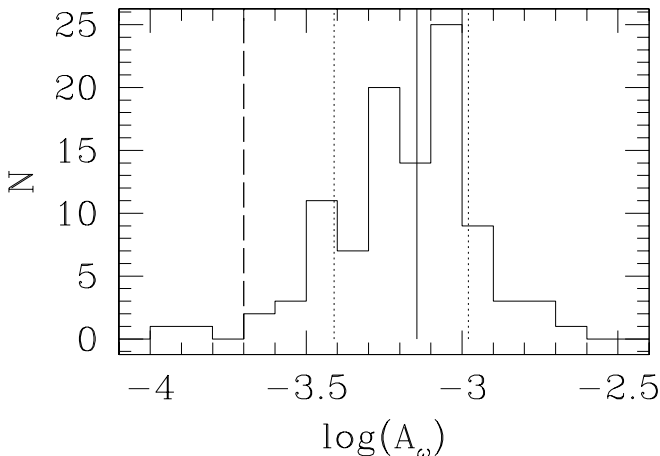


**Figure 6.** Histogram of fitted values of  $\log(A_\omega)$  carried out in 100 sub-samples of a  $1 \text{ deg}^2$  area containing  $\sim 4 \times 10^5$  particles, representing the surface density of objects in our  $B \sim 27.5$  sample. The solid line shows the median value of the histogram, dot-dashed lines illustrate the  $\pm 1\sigma$  confidence limits, and the dashed line shows the fitted value obtained from the WHDF.

similar growth of clustering. Combining Brainerd & Smail's three *I*- limited points with our own, we derive  $\epsilon = 0.70^{+0.70}_{-0.45}$ , again for  $r_0 = 4.3 h^{-1}$  Mpc.

We have also carried out a simulation similar to those described in Section 4.1 to see how secure is our rejection of the co-moving amplitude in the range  $B = 27 - 28$ , the results of which are presented in Figure 6. This simulation has the same galaxy number density as our observations at  $B \sim 27.5$  and covers an area of  $1 \text{ deg}^2$ . It contains a total of  $\sim 4 \times 10^5$  galaxies for an integral constraint  $C = 3.2$ . The simulation has  $\log(A_\omega) = -3.12 \pm 0.02$  (bootstrap errors), corresponding to the amplitude of our co-moving evolutionary model at this magnitude. Errors calculated by resam-

pling 100 WHDF-sized fields over this area gives a median  $\log(A_\omega) = -3.15^{+0.16}_{-0.26}$  ( $1\sigma$ ) and  $\log(A_\omega) = -3.15^{+0.36}_{-0.46}$  ( $2\sigma$ ). At  $B \sim 27$  we measure  $\log(A_\omega) = -3.7^{+0.13}_{-0.18}$  (bootstrap errors). Out of the 100 simulated fields, there are only two measurements at or below this value, leading us to conclude that in this magnitude range our measurement and the co-moving amplitude differs by at least  $2\sigma$ .

#### 5.4 The growth of clustering and biased galaxy formation

How does this observed rate of clustering growth compare with measurements from the literature? With deeper pencil-beam spectroscopic surveys, it has become possible to measure  $r_0$  at successively earlier epochs and to use this to infer a value for  $\epsilon$ . Using a statistically complete subsample of 591 galaxies from the Canada-France Redshift Survey (Lilly et al. 1995a), LeFevre et al. (1996) were able to measure the evolution of  $r_0$  in the interval  $0 \leq z \leq 1$ . They found  $r_0(z = 0.53) = 1.5 \pm 0.09 h^{-1}$  Mpc (for  $q_0 = 0.05$ ), implying  $0 < \epsilon < 2$ . Carlberg et al. (1997), using a sample of 248 galaxies, found that for  $M_K \leq -23.5$  galaxies,  $r_0(z \sim 0.6) = 2.0^{+0.9}_{-0.2} h^{-1}$  Mpc. At higher redshift, Carlberg et al. derive  $r_0(z \sim 0.97) = 1.4^{+0.9}_{-0.2} h^{-1}$  Mpc, which, combined with the lower redshift points from their survey, leads to  $\epsilon \sim 0.2 \pm 0.5$ . The Canadian Network for Observational Cosmology (CNOC) have recently completed a large field galaxy survey in the range  $0 \leq z \leq 0.7$  with a sample size of  $\sim 10^4$  galaxies (Carlberg et al. 1998). For luminous objects with corrected *R*-band absolute magnitudes of  $M_R^{k,e} < -20$  they find a slower clustering growth:  $\epsilon = -0.6 \pm 0.4$ , with  $r_0 = 5.15 \pm 0.15$ , strongly excluding clustering growth as rapid as  $\epsilon \sim 1$ .

The large size of the errors on our  $\chi^2$  fit does not permit us to make a detailed investigation of the dependence of  $\epsilon$  with sample selection. However, it is interesting that we find the rate of clustering growth to be slowest for our *K*- selected survey, and that our results are broadly consistent with those from the *K*- selected sample of Carlberg et al. (1997). We expect our *K*- selected galaxies to be good tracers of the underlying matter. *N*- body simulations (Colin, Carlberg, & Couchman 1997) have shown that in a low-density universe, the clustering of matter is expected to evolve as  $\epsilon \sim 0$ .

Our finding that  $0 > \epsilon > 2$ , is in agreement with the expectations from biased models of galaxy formation, which find that at the  $< 1 h^{-1}$  Mpc scales we are sensitive to, clustering growth is relatively rapid (Figure 1. of Baugh et al. (1999); Benson et al. (1999)). In comparison, at larger scales ( $\sim 5 h^{-1}$  Mpc) the correlation function evolves much more slowly. At such separations, the clustering pattern is "frozen in" as the galaxies are tracing higher-mass haloes whose clustering evolution is close to  $\epsilon = -1.2$ . In Figure 5 we see that that the predictions from the non-zero lambda cosmology fitted to the growth of clustering as observed in the simulation of Colin, Klypin, & Kravtsov (1999) is consistent with our observations and to the predictions of our  $\epsilon = 0$  model. The rapid decrease of the co-moving correlation length  $r_0$  between  $z = 0$  and  $z \sim 2$  for small haloes of  $V > 120 \text{ km s}^{-1}$  is a prediction of biased models which find faster clustering growth for intrinsically fainter galaxies. Even at brighter than  $B \sim 26$  our samples are dominated by  $\sim L^*$  galaxies (Metcalfe et al. 1996), unlike the Lyman-break galaxies of

Steidel et al. (1996) which higher intrinsic luminosities than this (The high resolution of Colin, Klypin, & Kravtsov's simulation and their adopted halo-finding algorithm makes it possible to locate haloes within haloes and therefore to successfully match the halo correlation function with the APM galaxy correlation function (Maddox et al. 1990a). For this reason we assume an approximate correspondence between these haloes and the intrinsically fainter galaxies which dominate our samples at  $B \sim 28$ .)

Figure 5 indicates that our observations are consistent with models displaying the non-monotonic dip in the  $r_0 - z$  relation, and illustrates why the "epsilon" models have been so successful in describing the observed scaling relation of  $\omega(\theta)$ . If our models are correct, even to  $B \sim 28$  the number of higher-redshift ( $z > 2.5$ , more highly clustered galaxies forms only a small fraction of total sample size (less than <5%) and this explains why scaling relations in which the galaxy correlation length decreases monotonically  $z \sim 1$  can successfully match the observations to  $B \sim 28$ .

## 6 CONCLUSIONS AND SUMMARY

In this paper we have presented a study of the projected two-point angular correlation function  $\omega(\theta)$  as measured in the WHDF and compared our measurements to results obtained from the much smaller North and South Hubble Deep Fields. The clustering amplitudes determined from the HDF are consistent with those in the WHDF, but none of our conclusions depend on our HDF measurements. In interpreting our results, we have used redshift distributions from a model which correctly predicts colours, number counts and redshift distributions for the faint galaxy population.

We find that at a fixed separation the amplitude of  $\omega(\theta)$  measured in *BRI* bandpasses is *lower* than the predictions of a low- $q_0$  model not containing luminosity evolution and in which clustering growth is stable in proper co-ordinates. For our  $K-$  selected samples, our correlation amplitudes are consistent with predictions from models having a low median redshift; we also find marginal evidence for a slower growth of clustering in these samples.

If our evolutionary models provide a correct description of the underlying redshift distributions (and comparisons to available observations at brighter magnitudes suggest they do), then our WHDF clustering measurements are consistent with a clustering growth  $0 > \epsilon > 2$  on the small scales ( $< 1h^{-1}$  Mpc) which we probe. We have also shown that this result is consistent with prediction of biased galaxy formation models which find faster clustering growth for intrinsically fainter galaxies like those which dominate our deep magnitude-limited surveys. We are able to use these rapid-growth "epsilon" models to successfully describe the clustering properties of our samples because the highly-clustered high-redshift galaxy population constitutes only a small fraction of the total galaxies observed in our survey.

Finally, our constant correlation amplitude found at  $B \sim 27 - 28$  is consistent with the expected reduction of cosmological volume element at high redshift and a steeper faint end slope for spiral galaxies, indicating that at these magnitude limits the median redshift of our sample ceases to increase.

## 7 ACKNOWLEDGEMENTS

H.J. McCracken wishes to thank Carlton Baugh, Ian Smail, Luigi Guzzo and Olivier LeFevre for careful readings of an earlier version of this manuscript. NM acknowledges partial PPARC support.

## REFERENCES

Adelberger K. L., Steidel C. C., Giavalisco M., Dickinson M., Pettini M., Kellogg M., 1998, ApJ, 505, 18  
 Barrow J. D., Sonoda D. H., Bhavsar S. P., 1984, MNRAS, 210, 19P  
 Baugh C. M., Benson A. J., Cole S., Frenk C. S., Lacey C. G., 1999, MNRAS, 305, L21  
 Baugh C. M., Gardner J. P., Frenk C. S., Sharples R. M., 1996, MNRAS, 283, L15  
 Benson A., Baugh C., Frenk C., Cole S., 1999, MNRAS, in preparation  
 Brainerd T. G., Smail I., 1998, ApJ, 494, L137  
 Brainerd T. G., Smail I., Mould J., 1994, MNRAS, 244, 408  
 Bruzual G., Charlot S., 1993, ApJ, 405, 538  
 Campos A., 1997, ApJ, 488, 606  
 Carlberg R. G., Cowie L. L., Songaila A., Hu E. M., 1997, ApJ, 484, 538  
 Carlberg R. G. et al., 1998, astro-ph/9805131  
 Colin P., Carlberg R. G., Couchman H. M. P., 1997, ApJ, 490, 1  
 Colin P., Klypin A., Kravtsov A. V., 1999, astro-ph/9907337  
 Colin P., Klypin A. A., Kravtsov A. V., Khokhlov A. M., 1999, ApJ, 523, 32  
 Cowie L. L., Songaila A., Hu E. M., 1996, AJ, 112, 839  
 Davis M., Peebles P. J. E., 1983, ApJ, 267, 465  
 Efstathiou G., Bernstein G., Katz N., Tyson J., Guhathakurta P., 1991, ApJ, 380, L47  
 Ellis R. S., Colless M., Broadhurst T., Heyl J., Glazebrook K., 1996, MNRAS, 280, 235  
 Giavalisco M., Steidel C. C., Adelberger K. L., Dickinson M. E., Pettini M., Kellogg M., 1998, ApJ, 503, 543  
 Glazebrook K., Ellis R., Colless M., Broadhurst T., Allington-Smith J., Tanvir N., 1995, MNRAS, 273, 157  
 Governato F., Baugh C. M., Frenk C. S., Cole S., Lacey C. G., Quinn T., Stadel J., 1998, Nat, 392, 359  
 Groth E. J., Peebles P. J. E., 1977, ApJ, 217, 385  
 Hamilton A. J. S., 1993, ApJ, 417, 19  
 Hudon J. D., Lilly S. J., 1996, ApJ, 469, 519  
 Infante L., Pritchett C. J., 1995a, ApJ, 439, 565  
 Infante L., Pritchett C. J., 1995b, ApJ, 439, 565  
 Jones L. R., Fong R., Shanks T., Ellis R. S., Peterson B. A., 1991, MNRAS, 249, 481  
 Jones L. R., Shanks T., Fong R., 1987, in High Redshift and Primeval Galaxies, eds Bergeron J., Kunth D., Rocca-Volmerange B., Tran Thanh Van J., Editions Frontieres, Gif-sur-Yvette, p.29, p. 29  
 Kauffmann G., Charlot S., 1998, MNRAS, 297, L23  
 Kauffmann G., Colberg J. M., Diaferio A., White S. D. M., 1999, MNRAS, 307, 529  
 Koo D. C., Szalay A. S., 1984, ApJ, 282, 390  
 Kravtsov A. V., Klypin A. A., 1999, ApJ, 520, 437  
 Kron R. G., 1980, ApJS, 43, 305  
 Landy S. D., Szalay A. S., 1993, ApJ, 412, 64  
 LeFevre O., Hudon D., Lilly S., Hammer F., Tresse L., 1996, ApJ, 461, 534  
 Lilly S. J., Cowie L. L., Gardner J. P., 1991, ApJ, 369, 79  
 Lilly S. J., Le Fevre O., Crampton D., Hammer F., Tresse L., 1995a, ApJ, 455, 50  
 Lilly S. J., Tresse L., Hammer F., Crampton D., Le Fevre O., 1995b, ApJ, 455, 108

Limber D. N., 1953, *ApJ*, 117, 134

Lin H., Yee H. K. C., Carlberg R. G., Ellingson E., 1997, *ApJ*, 475, 494

Lin H., Yee H. K. C., Carlberg R. G., Morris S. L., Sawicki M., Patton D. R., Wirth G., Shepherd C. W., 1999, *ApJ*, 518, 533

Ling E. N., Barrow J. D., Frenk C. S., 1986, *MNRAS*, 223, 21P

Loveday J., Maddox S. J., Efstathiou G., Peterson B. A., 1995, *ApJ*, 442, 457

Madau P., 1995, *ApJ*, 441, 18

Madau P., Ferguson H. C., Dickinson M. E., Giavalisco M., Steidel C. C., Fruchter A., 1996, *MNRAS*, 283, 1388

Maddox S. J., Efstathiou G., Sutherland W. J., Loveday J., 1990a, *MNRAS*, 242, 43P

Maddox S. J., Sutherland W. J., Efstathiou G., Loveday J., Peterson B. A., 1990b, *MNRAS*, 247, 1P

Marquardt D., 1963, *Journal of the Society for Industrial and Applied Mathematics*

McCracken H. J., Metcalfe N., Shanks T., Campos A., Gardner J. P., Fong R., 2000, *MNRAS*, 311, 707

Metcalfe N., Fong R., Shanks T., 1995, *MNRAS*, 274, 769

Metcalfe N., Shanks T., Campos A., Fong R., Gardner J. P., 1996, *Nat*, 383, 263

Metcalfe N., Shanks T., Campos A., McCracken H., Fong R., 2000, *MNRAS*, submitted

Metcalfe N., Shanks T., Fong R., Jones L. R., 1991, *MNRAS*, 249, 498

Metcalfe N., Shanks T., Fong R., Roche N., 1995, *MNRAS*, 273, 257

Neuschaefer L. W., Windhorst R. A., Dressler A., 1991, *ApJ*, 382, 32

Pei Y., 1992, *ApJ*, 395, 130

Pence W., 1976, *ApJ*, 203, 39

Phillipps S., Fong R., Fall S., Ellis R., Macgillivray H. T., 1978, *MNRAS*, 182, 673

Postman M., Lauer T. R., Szapudi I., Oegerle W., 1998, *ApJ*, 506, 33

Press W. H., Flannery B. P., Teukolsky S. A., Vetterling W. T., 1986, *Numerical Recipes*. Cambridge University Press

Pritchett C. J., Infante L., 1992, *ApJ*, 399, L35

Roche N., Eales S., Hippelein H., 1998, *MNRAS*, 295, 946

Roche N., Eales S. A., 1999, *MNRAS*, 307, 703

Roche N., Shanks T., Metcalfe N., Fong R., 1993, *MNRAS*, 263, 360

Roche N., Shanks T., Metcalfe N., Fong R., 1996, *MNRAS*, 280, 397

Schechter P., 1976, *apj*, 203, 297

Soneira R. M., Peebles P. J. E., 1978, *AJ*, 83, 845

Steidel C. C., Giavalisco M., Dickinson M., Adelberger K. L., 1996, *AJ*, 112, 352

Stevenson P. R. F., Shanks T., Fong R., Macgillivray H. T., 1985, *MNRAS*, 213, 953

Tucker D. L. et al., 1997, *MNRAS*, 285, L5

Villumsen J. V., Freudling W., Da Costa L. N., 1997, *ApJ*, 481, 578

Woods D., Fahlman G. G., 1997, *ApJ*, 490, 11